Supplementary information

Two Dimensional PdRuMoFeCo Multi-component Metallene for Rechargeable Zn-air Battery with High Performance

Fudong Li[#a], Yaojiang Zhou[#a], Qiuyu Zhang[a], Jiaxi Shu[a], Yuanmeng Zhao[a], Changsheng Shan[*a]

[a] Hubei Key Laboratory for Precision Synthesis of Small Molecule Pharmaceuticals, Collaborative Innovation Center for Advanced Organic Chemical Materials Co-constructed by the Province and Ministry, Ministry-of-Education Key Laboratory for the Synthesis and Application of Organic Functional Molecules, College of Chemistry and Chemical Engineering, Hubei University, Wuhan 430062, People's Republic of China.

[#] These authors contributed equally to this work.

[*] Corresponding author.

E-mail address:csshan@hubu.edu.cn

Experimental Section

1. Materials

Iron(III) acetylacetonate ($Fe(acac)_3$, 98%), Cobalt(III) acetylacetonate ($Co(acac)_3$, 98%), Palladium(II) acetylacetonate ($Pd(acac)_2$, 98%), Ruthenium(III) acetylacetonate ($Ru(acac)_3$, ≥99%) were purchased from Wuhan Changcheng Chemical Co. Ltd (China). Oleylamine (OAm, ≥80%), D-(+)-Glucose (99.5%) and Molybdenum hexacarbonyl ($Mo(CO)_6$, 98%) were purchased from Aladdin. Nafion solution (5%) was purchased from Sigma-Aldrich. Potassium hydroxide (KOH, 85%), ethanol (C_2H_6O) and cyclohexane (C_6H_{12}) were purchased from Sinopharm Chemical Reagent Co., Ltd. Commercial Pt/C (20 wt%) were purchased from Sigma-Aldrich. The deionized water is used in the experiment with a resistivity of 18.25 MΩ·cm.

2. Materials characterization.

X-ray diffraction (XRD) patterns were recorded using a Bruker D8 Advance diffractometer with Cu Kα radiation. Transmission electron microscopy (TEM). AFM image of the sample was conducted with (Bruker Dimension ICON). High-resolution transmission electron microscopy (HRTEM), scanning transmission electron microscopy (STEM) images, along with energy dispersive X-ray spectroscopy (EDS) data, were obtained using a JEOL JEM-2100F field emission transmission electron microscope equipped with an EDS spectrometer operating at 200 kV. X-ray photoelectron spectroscopy (XPS) data were collected on a Thermo Fisher Scientific ESCALAB 250Xi XPS system, with the binding energy of the C1s peak at 284.8 eV

used as a reference. Inductively coupled plasma optical emission spectrometer (ICP-OES) measurements were performed on an Agilent ICP-OES 725 analyzer.

3. Fabrication of PdRuMoFeCo Metallene.

The PdRuMoFeCo metallene was primarily synthesized via a wet-chemical method. First, 20 mL of oleylamine was heated at 100 ^{o}C for 30 min. Subsequently, the mixture of 62.0 mg of palladium acetylacetonate, 17.6 mg of iron acetylacetonate, 17.8 mg of cobalt acetylacetonate, 19.6 mg of ruthenium acetylacetonate, 13.2 mg of molybdenum hexacarbonyl, and 120 mg of glucose were added into the oleylamine and stirred for 10 min. Then, the mixture was placed in a high-pressure reactor and reacted at 350 ^{o}C for 2 h under 0.2 MPa high-purity CO gas. After that, the resulting product was washed by centrifugation and washing with a 4:1 mixture of ethanol and cyclohexane.

Pd metallene and quaternary alloy metallene reference samples (including RuMoFeCo, PdMoFeCo, PdRuFeCo, PdRuMoCo, and PdRuMoFe) were synthesized using the same procedure described above, with the only modification being the omission of the corresponding single metal precursor. To investigate compositional effects, PdxRuMoFeCo metallenes with tunable Pd contents and PdRuMoFeCox metallenes with tunable Co contents were also prepared following the identical protocol, except that varying amounts of palladium acetylacetonate (0, 31, 62, and 124 mg) or cobalt acetylacetonate (0, 8.9, 17.8, and 35.6 mg) were introduced during the reaction. In addition, PdRuMoFeCo nanoparticles were synthesized under otherwise

identical conditions, except that high-purity CO gas was not supplied during the reaction process.

4. Electrochemical measurements.

Firstly, 5 mg of the metallene/XC-72 carbon black (mass ratio of $m_{catalyst}$:$m_{carbon\ black}$=1:4) was dispersed by sonication in 1 mL of isopropanol solution with 0.05 wt% Nafion to form a homogeneous ink. A 5 mm diameter glassy carbon electrode (GCE) was polished with 0.05 μm γ alumina powder and then rinsed thoroughly with ultrapure water and ethanol.Then 10 μL of the ink was dropped onto the GCE surface at a catalyst loading of 0.2548 mg/cm² and air-dried before electrochemical measurements.

The electrochemical measurements were conducted in a three-electrode system on a CHI760E electrochemical station (Shanghai Chenhua Instrument Co., Ltd., China). A glassy carbon rotating disk electrode (GCRDE) with a diameter of 5 mm and a rotating ring-disk electrode with a GC disk and Pt ring (inner diameter: 6.25 mm; outer diameter: 7.92 mm) were employed as the working electrodes. A Pt foil electrode and a Hg/HgO electrode were used as the counter electrode and the reference electrode, respectively. Cyclic voltammetry (CV) tests were performed in an O_2-saturated 0.1 M KOH electrolyte at a scan rate of 5 mV/s. Nyquist plot by EIS spectra of different catalysts in 0.1 M KOH aqueous solution with a frequency range of 0.1 Hz to 100 kHz.The kinetic current (J_k) was calculated in accordance with the Koutecky-Levich equations (1) and (2). For rotating ring-disk electrode (RRDE) measurements, the electron transfer number (n) and the yield of the H_2O_2 intermediate (H_2O_2%) were calculated according to equations (3) and (4) below.

Where j represents the actual measured current density, j_K and j_L represent the diffusion current density and kinetic limiting current density, respectively, ω represents the angular velocity of the rotating electrode, F stands for Faraday's constant (96485 C mol^{-1}), C_0 denotes the volume concentration of oxygen $1.2*10^{-6}$ mol cm^{-3}, D_0 denotes the diffusion coefficient of oxygen $1.9*10^{-5}$ cm^{-2} s^{-1}, and ν is the kinematic viscosity of the electrolyte (ν=0.01 cm^{-2} s^{-1}). Where I_R stands for the actual measured ring current, I_D stands for the actual measured disk current, and □ is the current collection efficiency of the Pt ring (□ = 0.37).[1]

$$\frac{1}{j} = \frac{1}{j_k} + \frac{1}{j_L} = \frac{1}{j_k} + 1/(B\omega^{\frac{1}{2}}) \quad (1)$$

$$B = 0.62nFC_0D_0^{2/3}v^{-1/6} \quad (2)$$

$$H_2O_2\% = 200 * \frac{I_R/N}{I_D * I_R/N} \quad (3)$$

$$n = 400 * \frac{I_R/N}{I_D * I_R/N} \quad (4)$$

5. Zinc-air battery measurements

The catalyst ink was drop-coated onto a nickel-foam substrate to serve as the air cathode with an area of 1 cm^2 and a loading of 0.5 mg cm^{-2}. A polished zinc flake was employed as the anode of the zinc-air battery. A solution of 6 M KOH and 0.2 M Zn $(CH_3COO)_2$ was used as the battery electrolyte. After assembling the components into a rechargeable zinc-air battery at 25 °C, the battery performance was tested using the Sunway battery test system.

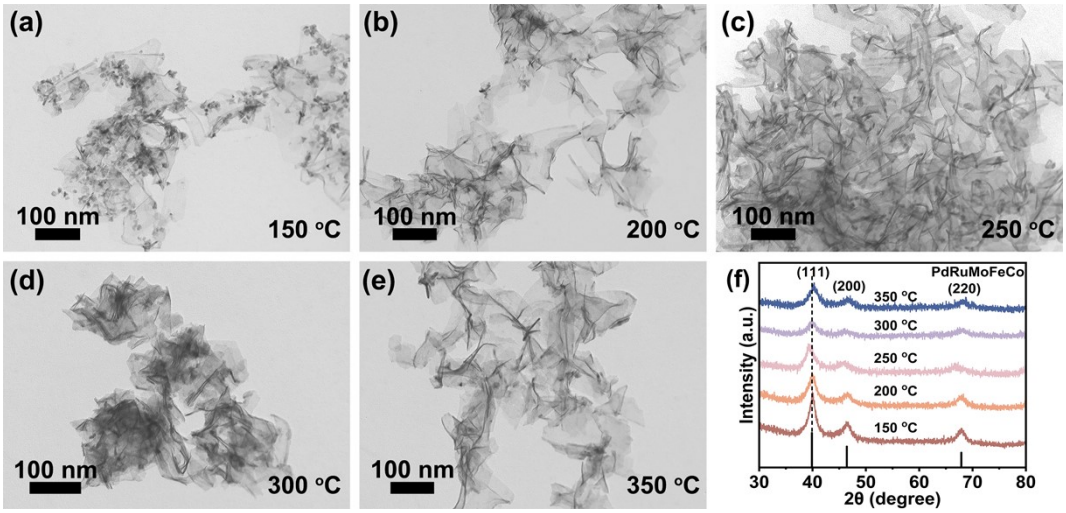

Figure S1. TEM images (a-e) and XRD patterns (f) of PdRuMoFeCo metallenes at different reaction temperatures of 150 °C, 200 °C, 250 °C, 300 °C and 350 °C.

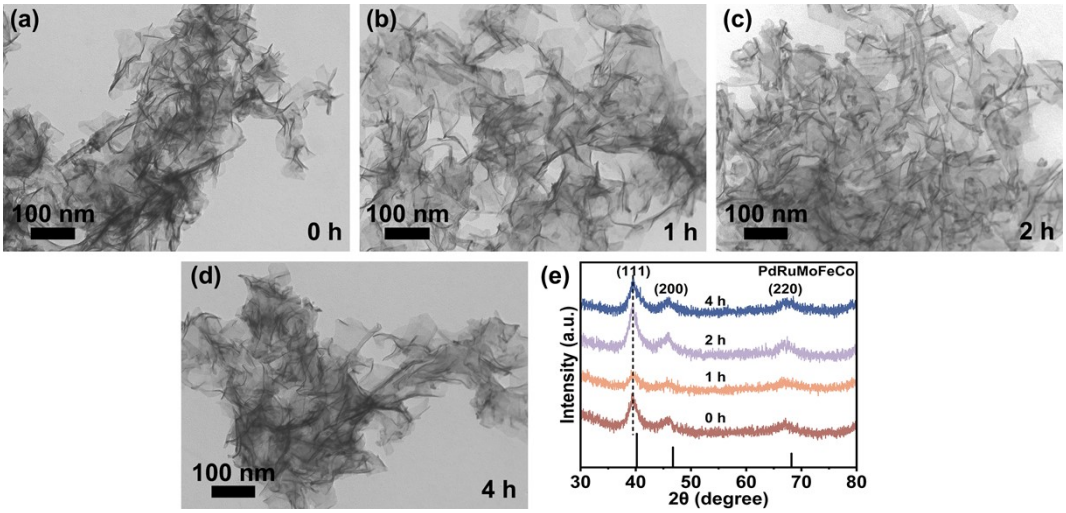

Figure S2. TEM images (a-d) and XRD patterns (e) of PdRuMoFeCo metallenes with different reaction times of 0 h, 1 h, 2 h and 4 h.

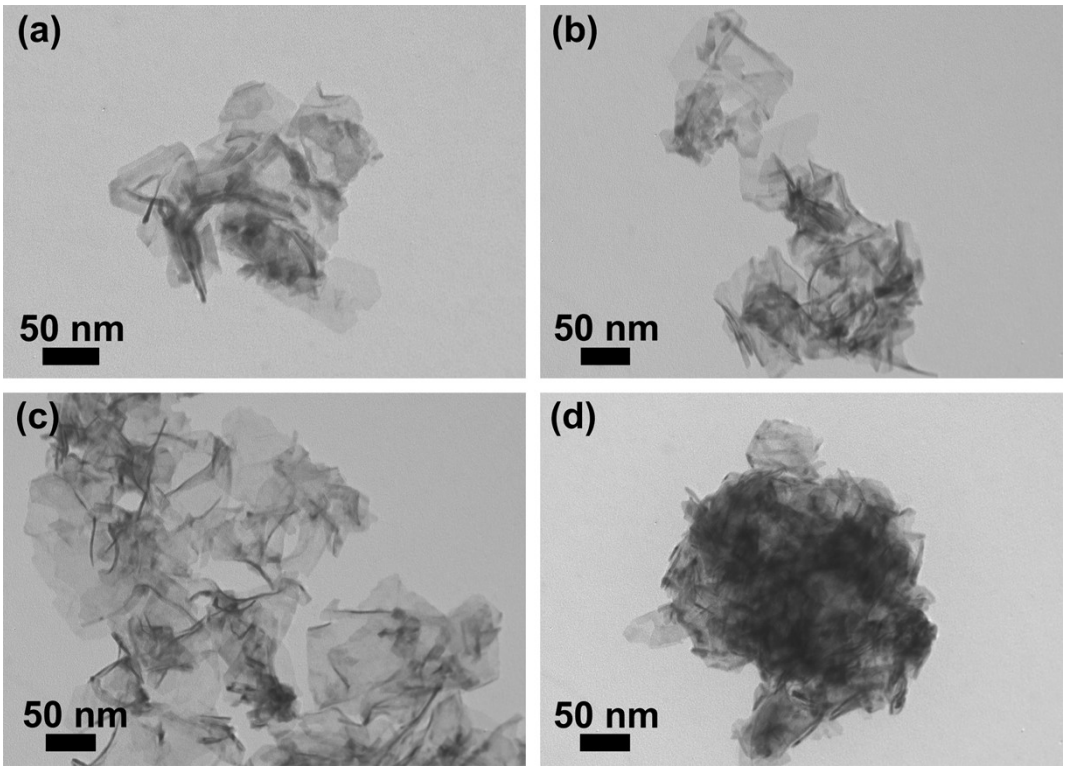

Figure S3. TEM images of quaternary metallenes, including PdRuFeCo (a), PdRuMoFe (b), PdRuMoCo (c) and PdMoFeCo (d).

TEM characterization shows that all of the quaternary metallenes PdRuFeCo, PdRuMoFe, PdRuMoCo, and PdMoFeCo show the morphology of nanosheet.

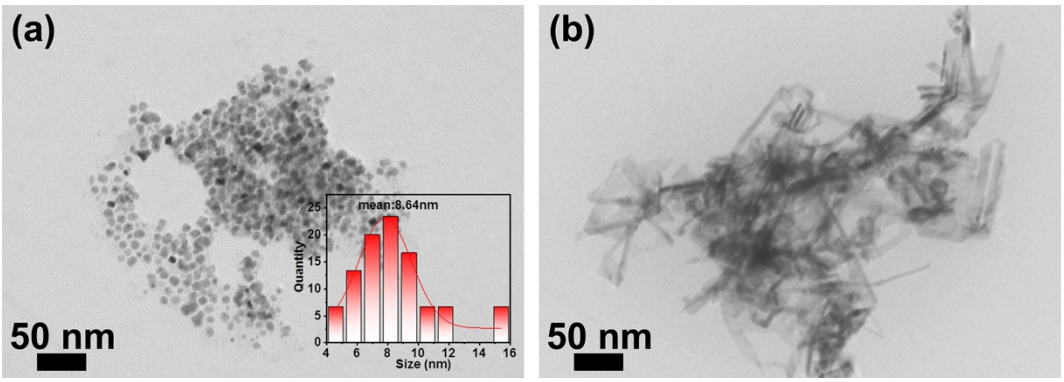

Figure S4. (a). TEM images of PdRuMoFeCo-NPs (a) and Pd metallene (b).

Control samples of PdRuMoFeCo nanoparticles (NPs) and pure Pd metallene were synthesized. TEM images demonstrated the nanoparticle morphology of PdRuMoFeCo-NPs with an average size of 8.64 nm, while the Pd metallene maintains the morphology of nanosheet.

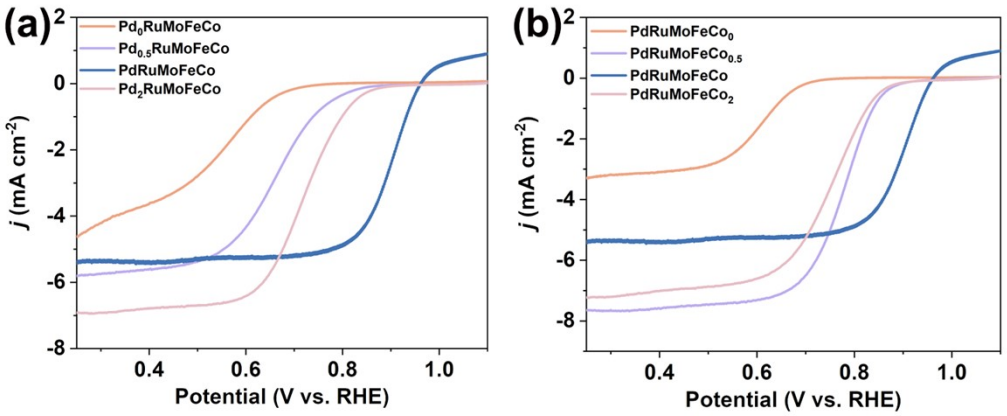

Figure S5. LSV curves of PdRuMoFeCo metallene prepared with different dosages of (a) palladium acetylacetonate (0 mg, 31 mg, 62 mg, 124 mg) and (b) cobalt acetylacetonate (0 mg, 8.9 mg, 17.8 mg, 35.6 mg) for ORR.

Each catalyst was synthesized via the identical procedure except different dosages of the cobalt and palladium metal precursors.

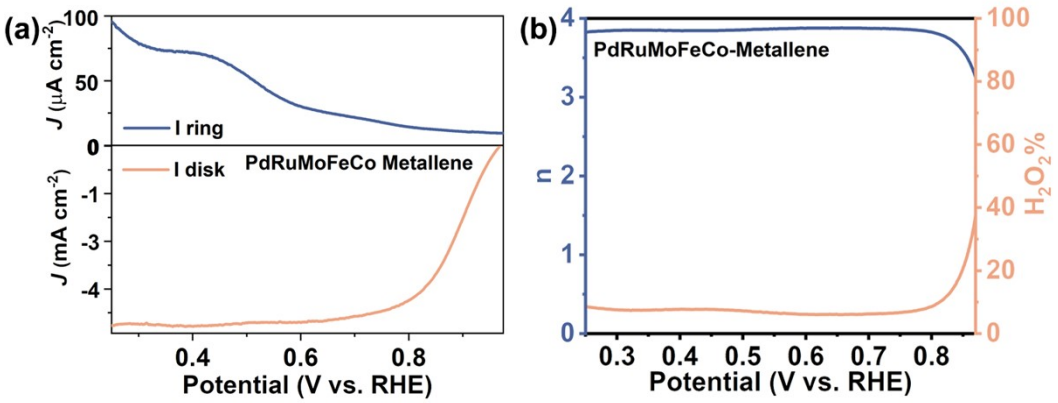

Figure S6. (a) RRDE voltammograms of the PdRuMoFeCo metallene in oxygen-saturated 0.1 M KOH solution with a rotation speed of 1600 rpm and scan rate of 10 mV s^{-1}. (b) Electron transfer number (n) and hydrogen peroxide yield (H_2O_2%) of PdRuMoFeCo metallene for ORR at 1600 rpm.

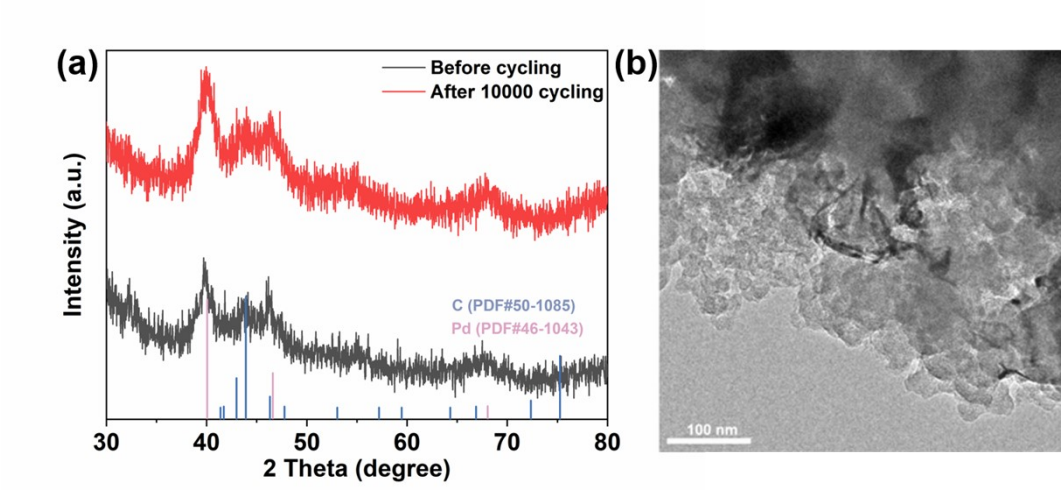

Figure S7. (a) XRD patterns of PdRuMoFeCo metallene/C before and after 10,000 cycles of cyclic voltammetry; (b) TEM image of the PdRuMoFeCo metallene/C after 10, 000 cycling.

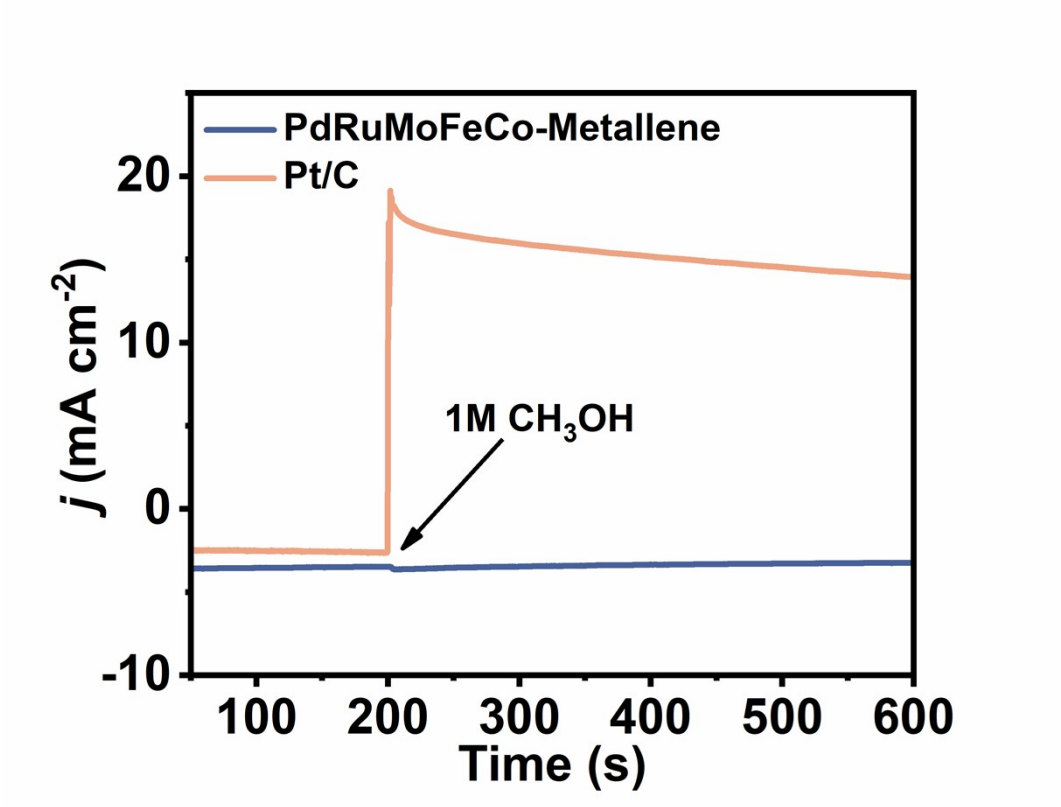

Figure S8. Methanol tolerance tests of PdRuMoFeCo metallene and Pt/C.

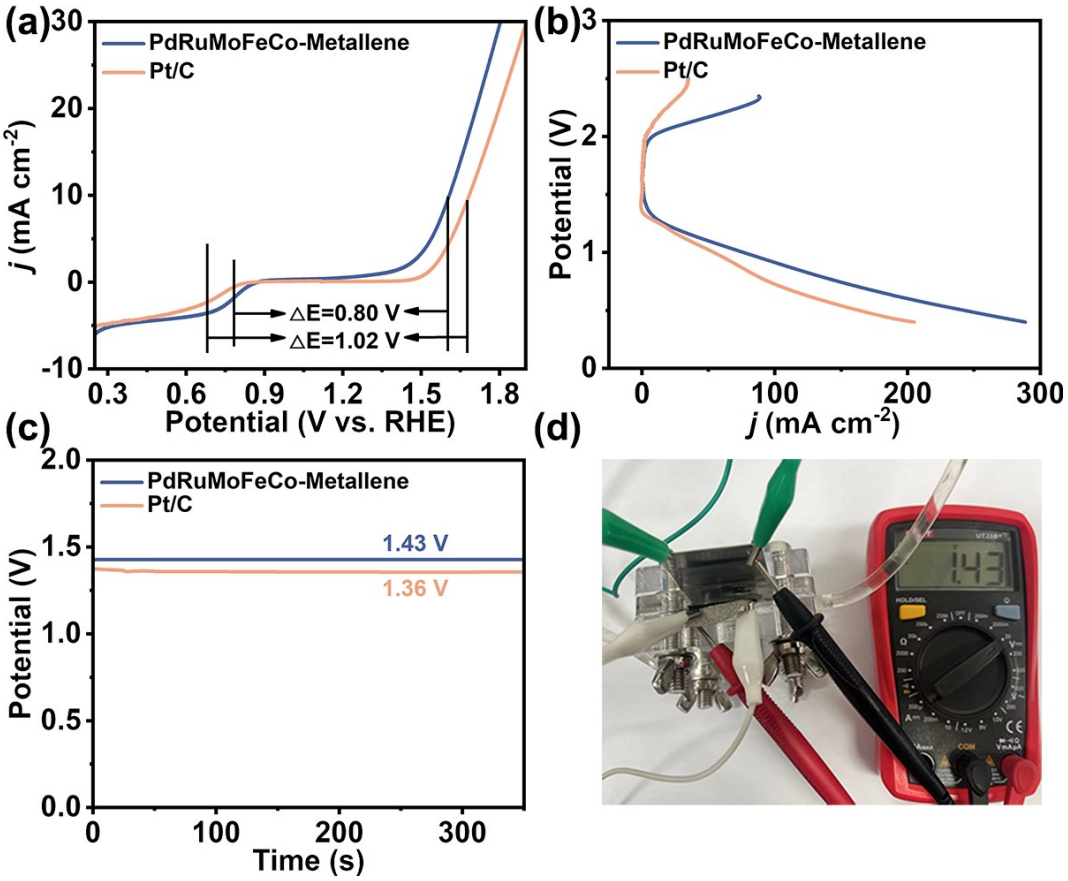

Figure S9. (a) LSV curves of as-prepared catalysts for bifunctional catalytic activities of ORR and OER. (b) Charge and discharge polarization curves of PdRuMoFeCo metallene and Pt/C based zinc-air batteries. (c) Open current-voltage curves using Pt/C and PdRuMoFeCo metallene based zinc-air batteries. (d) Picture of open circuit voltage test.

Table S1. Weight percentages of metal elements in different catalysts measured by ICP-AES.

Samples	Pd（wt%）	Ru（wt%）	Mo（wt%）	Fe（wt%）	Co（wt%）
PdRuMoFeCo-metallene	64.80	14.49	4.21	12.24	4.26
PdRuMoFeCo-NPs	78.75	6.34	2.72	8.36	3.83
PdRuMoFe	79.72	2.06	0.71	17.51	--

Table S2. Comparison of ORR performance of PdRuMoFeCo metallene in this work with those in previously reported works in 0.1 M KOH solution.

Materials	**E_{onset} (V vs. RHE)**	**$E_{1/2}$ (V vs. RHE)**	**Ref**
PdRuMoFeCo metallene	0.966	0.893	This Work
AlNiCoRuMo	0.99	0.875	[2]
$Ru_{0.2}Co_{2.8}O_4$	0.88	0.77	[3]
Pd-Ru@NG	0.92	0.81	[4]
FeNi/N-CPCF-950	0.99	0.867	[5]
CrMnFeCoNi	0.88	0.78	[6]
AlFeCoNiCr	/	0.71	[7]
$Pt_{34}Fe_5Ni_{20}Cu_{31}Mo_9Ru$	/	0.87	[8]
$(AlNiCoFeCr)_3O_4$/Ag	/	0.81	[9]

Table S3. Comparison of zinc-air battery performance based on PdRuMoFeCo metallene in this work with those in previously reported works.

Catalysts	Catalyst loading (mg/cm^2)	OCV (V)	Energy density (mAh/g; J=10 mA/cm^2)	Peak power density (mW/cm^2; J=10 mA/cm^2)	Ref.
PdRuMoFeCo metallene	0.50	1.430	787.6	175.30	This work
Co_2P/CoN_4@NSC-500	1.25	1.450	971.0 (J=5)	134.49	[10]
Fe_3C/Fe-N-C	1.00	1.414	/	63.00	[11]
Fe-Ni@NDC	1.00	1.461	763.0	270.00	[12]
HPFe-N-C	2.00	1.476	672.0	160.00	[13]
Fe_3C@NPW	1.00	1.480	804.0	125.00	[14]
PdNi/Ni@N-C	/	1.410	719.2 (J=5)	108.50	[15]
Fe-N_4/Pt-N_4@NC	1.00	1.480	749.8	200.00	[16]
SA-PtCoF	0.42	1.310	808.0	125.00	[17]
Pt-SCFP/C-12	2.00	1.440	781.5	122.00	[18]
Fe-N/P-C-700	3.00	1.420	723.6 (J=100)	133.20	[19]
PdMo Metallene/C	1.00	1.483	798.0	154.20	[20]
$Fe_{12}Ni_{23}Cr_{10}Co_{30}Mn_{25}$/CNT	/	1.400	760.0	128.60	[21]
PtPdAuAgCuIrRu	0.50	1.528	/	146.40	[22]
AlNiCoRuMoCrFeTi oxide	0.50	1.512	/	123.50	[23]
$Pt_{34}Fe_5Ni_{20}Cu_{31}Mo_9Ru$	1.00	/	/	150.00	[8]

References

1 A. Han, X. Wang, K. Tang, Z. Zhang, C. Ye, K. Kong, H. Hu, L. Zheng, P. Jiang, C. Zhao, Q. Zhang, D. Wang and Y. Li, *Angew. Chem. Int. Ed.*, 2021, **133**, 19411–19420.

2 Z. Jin, J. Lyu, Y.-L. Zhao, H. Li, X. Lin, G. Xie, X. Liu, J.-J. Kai and H.-J. Qiu, *ACS Mater. Lett.*, 2020, **2**, 1698–1706.

3 S. Guo, R. Bao, S. Li, Y. Ye, E. Zhu, W. Wang, Y. Zhang, H. Chen and Y. Ye, *J. of Alloys and Compd.*, 2020, **827**, 154269.

4 B. K. Barman, B. Sarkar and K. K. Nanda, *Chem. Commun.*, 2019, **55**, 13928–13931.

5 Z. Wang, J. Ang, J. Liu, X. Y. D. Ma, J. Kong, Y. Zhang, T. Yan and X. Lu, *Appl. Catal. B Environ.Energy.*, 2020, **263**, 118344.

6 R. He, L. Yang, Y. Zhang, X. Wang, S. Lee, T. Zhang, L. Li, Z. Liang, J. Chen, J. Li, A. Ostovari Moghaddam, J. Llorca, M. Ibáñez, J. Arbiol, Y. Xu and A. Cabot, *Energy Storage Mater.*, 2023, **58**, 287–298.

7 G. Fang, J. Gao, J. Lv, H. Jia, H. Li, W. Liu, G. Xie, Z. Chen, Y. Huang, Q. Yuan, X. Liu, X. Lin, S. Sun and H.-J. Qiu, *Appl. Catal. B Environ. Energy*, 2020, **268**, 118431.

8 Z. Chen, J. Wen, C. Wang and X. Kang, *Small*, 2022, **18**, 2204255.

9 Y. Zhang, J. Lyu, Y.-L. Zhao, K. Hu, Z. Chen, X. Lin, G. Xie, X. Liu and H.-J. Qiu, *Nanoscale*, 2021, **13**, 16164–16171.

10 Y. Zhao, J. Wen, P. Li, P. Zhang, S. Wang, D. Li, J. Dou, Y. Li, H. Ma and L. Xu,

Angew. Chem. Int. Ed., 2023, **62**, e202216950.

11 Y. Chen, X. Kong, Y. Wang, H. Ye, J. Gao, Y. Qiu, S. Wang, W. Zhao, Y. Wang, J. Zhou and Q. Yuan, *Chem. Eng. J.*, 2023, **454**, 140512.

12 Z. Nie, M. Chen, L. Zhang, Q. Feng, J. Hu, X. Huang, C. Zhou, Y. Zhou, T. Wågberg and G. Hu, *Chem. Eng. J.*, 2023, **463**, 142411.

13 H. Xu, D. Wang, P. Yang, L. Du, X. Lu, R. Li, L. Liu, J. Zhang and M. An, *Appl. Catal. B Environ. Energy*, 2022, **305**, 121040.

14 M. Cao, Y. Liu, K. Sun, H. Li, X. Lin, P. Zhang, L. Zhou, A. Wang, S. Mehdi, X. Wu, J. Jiang and B. Li, *Small*, 2022, **18**, 2202014.

15 Z. Li, H. Li, M. Li, J. Hu, Y. Liu, D. Sun, G. Fu and Y. Tang, *Energy Storage Mater.*, 2021, **42**, 118–128.

16 A. Han, X. Wang, K. Tang, Z. Zhang, C. Ye, K. Kong, H. Hu, L. Zheng, P. Jiang, C. Zhao, Q. Zhang, D. Wang and Y. Li, *Angew. Chem. Int. Ed.*, 2021, **133**, 19411–19420.

17 Z. Li, W. Niu, Z. Yang, N. Zaman, W. Samarakoon, M. Wang, A. Kara, M. Lucero, M. V. Vyas, H. Cao, H. Zhou, G. E. Sterbinsky, Z. Feng, Y. Du and Y. Yang, *Energy Environ. Sci.*, 2020, **13**, 884–895.

18 X. Wang, J. Sunarso, Q. Lu, Z. Zhou, J. Dai, D. Guan, W. Zhou and Z. Shao, *Adv. Energy Mater.*, 2020, **10**, 1903271.

19 K. Yuan, D. Lützenkirchen-Hecht, L. Li, L. Shuai, Y. Li, R. Cao, M. Qiu, X. Zhuang, M. K. H. Leung, Y. Chen and U. Scherf, *J. Am. Chem. Soc.*, 2020, **142**, 2404–2412.

20 M. Luo, Z. Zhao, Y. Zhang, Y. Sun, Y. Xing, F. Lv, Y. Yang, X. Zhang, S. Hwang, Y. Qin, J.-Y. Ma, F. Lin, D. Su, G. Lu and S. Guo, *Nature*, 2019, **574**, 81–85.

21 X. Cao, Y. Gao, Z. Wang, H. Zeng, Y. Song, S. Tang, L. Luo and S. Gong, *ACS Appl. Mater. Interfaces*, 2023, **15**, 32365–32375.

22 Z. Jin, X. Zhou, Y. Hu, X. Tang, K. Hu, K. M. Reddy, X. Lin and H.-J. Qiu, *Chem. Sci.*, 2022, **13**, 12056–12064.

23 Z. Jin, J. Lyu, K. Hu, Z. Chen, G. Xie, X. Liu, X. Lin and H. Qiu, *Small*, 2022, **18**, 2107207.